AIAA JOURNAL
Vol. 43, No. 3, March 2005

Modeling the Effect of Shock Unsteadiness in Shock/Turbulent Boundary-Layer Interactions

Krishnendu Sinha,* Krishnan Mahesh,† and Graham V. Candler‡
University of Minnesota, Minneapolis, Minnesota 55455

Reynolds-averaged Navier–Stokes (RANS) methods often cannot predict shock/turbulence interaction correctly. This may be because RANS models do not account for the unsteady motion of the shock wave that is inherent in these interactions. Previous work proposed a shock-unsteadiness correction that significantly improves prediction of turbulent kinetic energy amplification across a normal shock in homogeneous isotropic turbulence. We generalize the modification to shock-wave/turbulent boundary-layer interactions and implement it in the k–ϵ, k–ω, and Spalart–Allmaras models. In compression-corner flows, the correction decreases the turbulent kinetic energy amplification across the shock compared to the standard k–ϵ and k–ω models. This results in improved prediction of the separation shock location, delayed reattachment, and slower recovery of the boundary layer on the ramp. For the Spalart–Allmaras model, the modification amplifies eddy viscosity across the shock, moving the separation location closer to the experiment.

Nomenclature

b_1'	=	shock-unsteadiness model coefficient
c_f	=	skin friction coefficient
k	=	turbulent kinetic energy
M_{1n}	=	upstream Mach number normal to a shock
P_k	=	production of turbulent kinetic energy
p	=	pressure
Re_t	=	turbulent Reynolds number
S_{ij}	=	symmetric part of mean strain rate tensor
$\tilde{u}$	=	Favre-averaged velocity
δ_0	=	boundary-layer thickness upstream of interaction
ϵ	=	turbulent dissipation rate
μ	=	molecular viscosity
μ_T	=	turbulent eddy viscosity
ν_T	=	turbulent kinematic viscosity
$\bar{\rho}$	=	mean density
ω	=	specific dissipation rate

Subscripts

n	=	direction normal to a shock
w	=	conditions at a wall
1, 2	=	upstream, downstream of a shock wave
∞	=	freestream

Introduction

THE characteristics of a turbulent boundary layer in a supersonic flow can be drastically altered by a shock wave. The interaction can lead to high pressure and heat loads, as well as regions of separated flow. These play an important role in the design and operation of high-speed aerospace vehicles and propulsion systems. Commonly studied flow configurations include compression ramps, oblique shocks impinging on boundary layers, transonic airfoils, and single or double fins on plates.

Engineering prediction of shock-wave/turbulent boundary-layer interaction relies on Reynolds-averaged Navier–Stokes (RANS) simulations. However, significant disagreement with experimental data is observed, especially in the presence of strong shock waves.[1,2] For example, in compression corner flows with high deflection angle, conventional RANS models cannot predict the location of the separation shock, size of the separation region at the corner, and mean velocity profiles downstream of the interaction.[2,3] Several modifications have been proposed to improve predictions, e.g., realizability constraint,[2] compressibility correction,[3,4] length-scale modification,[4] and rapid compression correction.[4] The outcome of the modifications vary from model to model, and also vary with test conditions. The flowfield generated by the interaction of shock wave with a turbulent boundary layer is inherently unsteady. However, turbulence models used in RANS methods do not account for the unsteady motion of the shock. This is identified as one of the main reasons for their poor performance in strong shock-wave/turbulent boundary-layer interactions.[5]

Sinha et al.[6] study the interaction of homogeneous isotropic turbulence with a normal shock in the RANS framework. They show that the standard k–ϵ model[7] with compressibility corrections[8,9] overpredicts the turbulent kinetic energy behind the shock. Eddy viscosity corrections based on the realizability constraint are shown to improve results but still do not correctly predict k behind the shock. Sinha et al.[6] also identify a damping mechanism caused by the coupling between shock motion and turbulent fluctuations in the incoming flow. A model is proposed for this shock-unsteadiness effect, based on an analysis of the linearized conservation equations that govern shock/homogeneous turbulence interaction. The model predicts the evolution of turbulent kinetic energy across the shock accurately. However, it is strictly applicable only when the mean flow on either side of the shock is uniform. The current paper generalizes the shock-unsteadiness model[6] to flows with additional mean gradients. It is then applied to interaction of turbulent boundary layers with shock waves.

The paper is organized as follows. First, the mean flow equations and the k–ϵ, k–ω, and Spalart–Allmaras (SA) turbulence models are summarized. This is followed by the implementation of the shock-unsteadiness correction[6] to these models. Next, the numerical method used to solve the conservation equations is described, along with the boundary conditions used in the simulations. Finally, the results obtained for the compression corner flows are presented. Ramp angles of 24, 20, and 16 deg are considered, and the model predictions are compared to experimental data of Settles and Dodson.[10]

Presented as Paper 2004-1129 at the 42nd Aerospace Sciences Meeting, Reno, NV, 5–8 January 2004; received 26 February 2004; revision received 3 September 2004; accepted for publication 8 September 2004.

*Research Associate, Department of Aerospace Engineering and Mechanics, 110 Union Street SE. Member AIAA.
†Assistant Professor, Department of Aerospace Engineering and Mechanics. Member AIAA.
‡Professor, Department of Aerospace Engineering and Mechanics. Associate Fellow AIAA.

Simulation Methodology

We solve the two-dimensional Favre-averaged Navier–Stokes equations for the mean flow, as presented in Ref. 11. The k–ω model of Wilcox,[12] the low-Reynolds-number k–ϵ model of Launder and Sharma,[7] and the Spalart–Allmaras (SA) model[13] are used for turbulence closure. The modeled transport equations for k, ϵ, and ω are given in Refs. 7 and 12. The Spalart–Allmaras model[13] solves a transport equation for $\bar{\rho}\tilde{\nu}$, where $\tilde{\nu}$ is related to ν_T via a wall damping function. Note that the conserved variable in the energy equation used with the Spalart–Allmaras model does not include the turbulent kinetic energy.

Shock-Unsteadiness Modification to the k–ϵ and k–ω Models

In the k–ϵ model, the production of k is given by

$$P_k = \mu_T\left(2S_{ij}S_{ji} - \tfrac{2}{3}S_{ii}^2\right) - \tfrac{2}{3}\bar{\rho}kS_{ii} \tag{1}$$

In a shock wave, the production is proportional to S_{ii}^2, which is very large in magnitude. This results in excessively high values of k behind the shock.[6] The production of k in the k–ω model is identical to that in Eq. (1), and therefore it also overly amplifies k across the shock. Here, $S_{ij} = \frac{1}{2}(\partial\tilde{u}_i/\partial x_j + \partial\tilde{u}_j/\partial x_i)$ and $\tilde{u}_i$ is the component of the Favre-averaged velocity in the x_i direction. In the k–ω model $\mu_T = \bar{\rho}k/\omega$, and in the k–ϵ formulation $\mu_T = c_\mu f_\mu \bar{\rho}k^2/\epsilon$, where $c_\mu = 0.09$, $f_\mu = \exp(-3.4/(1+0.02Re_t)^2)$ is a damping function, and $Re_t = \bar{\rho}k^2/\mu\epsilon$.

Sinha et al.[6] argue that the eddy viscosity assumption breaks down in the highly nonequilibrium flow through a shock, and a more accurate amplification of k is obtained by setting $\mu_T = 0$ in Eq. (1). They also note that unsteady shock motion damps the amplification of k across a shock. Based on linear analysis results, they propose the following modification to the production term in a shock wave:

$$P_k = -\tfrac{2}{3}\bar{\rho}kS_{ii}(1 - b_1') \tag{2}$$

where

$$b_1' = \max[0,\, 0.4(1 - e^{1-M_{1n}})] \tag{3}$$

represents the damping effect caused by the coupling between the shock unsteadiness and the upstream velocity fluctuations. Here, M_{1n} is measured in a frame of reference that is stationary with respect to the shock wave. The model is shown to accurately predict the amplification of k in shock/homogeneous turbulence interactions.[6] Note that the expression for b_1' in Eq. (3) is modified from its original form[6] to ensure that the shock-unsteadiness modification is not applied when $M_{1n} < 1$.

The amount of turbulence in a boundary layer directly affects flow separation in an adverse pressure gradient. Higher turbulence levels delay separation, which may explain why simulations using the standard k–ω and k–ϵ models predict later separation than is observed in experiments.[2,14] Lower production of k in the shock due to the shock-unsteadiness effect is therefore expected to improve results. To match the production of k in the shock to the value prescribed by Eq. (2), we replace μ_T in Eq. (1) by $c_\mu'\mu_T$, where

$$c_\mu' = 1 - f_s\left[1 + \left(b_1'/\sqrt{3}\right)/\zeta\right] \tag{4}$$

for the k–ω model. Here $\zeta = S/\omega$ is a dimensionless mean strain rate, and $S = [2S_{ij}S_{ji} - \frac{2}{3}S_{ii}^2]^{1/2}$. For the k–ϵ model,

$$c_\mu' = 1 - f_s\left[1 + \left(b_1'/\sqrt{3}\right)/\zeta c_\mu f_\mu\right] \tag{5}$$

where $\zeta = Sk/\tilde{\epsilon}$ and $\tilde{\epsilon} = \epsilon + 2\nu(\partial\sqrt{k}/\partial x_j)^2$ is the total dissipation rate obtained by adding the low-Reynolds-number term in the k-equation to the turbulent dissipation rate.[7] Here f_s is an empirical function that identifies the region of the shock wave in terms of the ratio S_{ii}/S:

$$f_s = \tfrac{1}{2} - \tfrac{1}{2}\tanh(5S_{ii}/S + 3) \tag{6}$$

such that $f_s = 1$ in regions of high compression and $f_s = 0$ otherwise.

The shock-unsteadiness modification is applied only to the k-equation. All other governing equations, including ϵ and ω equations, remain unchanged. The conservation equation for total energy includes contribution for the mean flow and the turbulence field. The shock-unsteadiness model alters the transfer between the mean and turbulent kinetic energies and therefore does not affect the overall conservation of the total energy. Also, note that the solutions obtained using these models are steady and the modification accounts for an averaged effect of shock unsteadiness.

Shock-Unsteadiness Modification to SA Model

In the SA model, the mean flow influences the turbulence field via the production term that is a function of the mean vorticity. Therefore, the eddy viscosity is insensitive to mean dilatation in a shock wave. However, the mean vorticity field in a turbulent boundary layer changes across a shock wave. This can alter the production term and thus can change $\tilde{\nu}$ in the vicinity of the shock. In a 24-deg compression corner flow, for example, the interaction of the turbulent boundary layer with the oblique shock results in a small increase in $\tilde{\nu}$ (less than 5% of the local $\tilde{\nu}$ magnitude).

Interaction with a shock wave enhances the turbulent fluctuations in a flow. Sinha et al.[6] propose the following model for the amplification of k and ϵ across a shock wave:

$$k_2/k_1 = (\tilde{u}_{n,1}/\tilde{u}_{n,2})^{\frac{2}{3}(1-b_1')}, \qquad \epsilon_2/\epsilon_1 = (\tilde{u}_{n,1}/\tilde{u}_{n,2})^{\frac{2}{3}c_{\epsilon 1}}$$

where b_1' represents the effect of the shock-unsteadiness, given by (3), and $c_{\epsilon 1} = 1.25 + 0.2(M_{1n} - 1)$. Noting that $\nu_T \propto k^2/\epsilon$, the change in ν_T or $\tilde{\nu}$ across a shock can be estimated as

$$\tilde{\nu}_2/\tilde{\nu}_1 = (k_2/k_1)^2(\epsilon_1/\epsilon_2) = (\tilde{u}_{n\cdot 1}/\tilde{u}_{n,2})^{c_{b1}'}$$

where $c_{b1}' = \frac{4}{3}(1 - b_1') - \frac{2}{3}c_{\epsilon 1}$. This can be achieved by a production term of the form $-c_{b1}'\bar{\rho}\tilde{\nu}S_{ii}$ in the transport equation for $\bar{\rho}\tilde{\nu}$. Note that this additional term is effective only in regions of strong compression and therefore does not alter the standard SA model elsewhere.

Numerical Method

The governing equations are discretized in a finite volume formulation where the inviscid fluxes are computed using a modified (low-dissipation) form of the Steger–Warming flux-splitting approach.[15] The turbulence model equations are fully coupled to the mean flow equations. The details of the formulation are given in Ref. 16. The method is second-order accurate in both streamwise and wall-normal directions. The viscous fluxes and the turbulent source terms are evaluated using a second-order-accurate central difference method. The implicit data parallel line relaxation method of Wright et al.[17] is used to obtain steady-state solutions.

Boundary Conditions

Inlet profiles for the computations are obtained from separate flat plate simulations using the standard k–ω, k–ϵ, and SA models discussed earlier. The value of the momentum thickness reported in the experiments[10] is matched to obtain the mean flow and turbulence profiles at the inlet boundary of the compression ramp simulations.

Nominal test section conditions reported in the experiments are specified in the freestream, and a no-slip isothermal boundary condition (based on wall temperature measurements) is applied on solid walls. For the turbulence model equations, the boundary conditions at the wall are $k = 0$, $\epsilon = 0$, $\tilde{\nu} = 0$, and $\omega = 60\nu_w/\beta\Delta y_1^2$, where ν_w is the kinematic viscosity at the wall, $\beta = 3/40$ is a model constant, and Δy_1 is the distance to the next point away from the wall. Following Menter,[18] the freestream conditions used for the flat plate simulations using the k–ω model are

$$\omega_\infty = 10U_\infty/L, \qquad k_\infty = 0.01\,\nu_\infty\omega_\infty$$

where $L = 1$ m is a characteristic length of the plate and the subscript ∞ denotes the freestream conditions. In the case of the k–ϵ and SA

models,

$$k_\infty = 0.002\,U_\infty^2, \qquad \epsilon_\infty = 0.1 c_\mu \bar{\rho}_\infty k_\infty^2 \big/ \mu_\infty, \qquad \tilde{\nu}_\infty = 0.1\mu_\infty/\bar{\rho}_\infty$$

are used in the freestream.[13,18] For the compression ramp simulations, k, ϵ, ω, and $\tilde{\nu}$ values at the boundary-layer edge in the inlet profile are prescribed as the freestream conditions at the top boundary. An extrapolation condition is used at the exit boundary of the domain.

Test Cases and Grid Refinement Study

We compute the three compression ramp flows listed in Table 1. The computational domain consists of a 10-cm flat plate followed by a 15-cm-long ramp and extends to 5 cm above the plate at the inlet location. The grids for the k–ω and SA simulations consist of 120 equispaced points in the streamwise direction and 110 exponentially stretched points in the wall normal direction. The first point is located 0.001 mm from the wall, which is equivalent to 0.6 wall units or less along the solid wall. A grid refinement study was performed for all three test cases and the results for the 24-deg compression corner are shown in Figs. 1 and 2. The pressure and skin friction coefficient obtained on a finer grid (240×200) are almost identical to those obtained on the base grid (120×110). The skin friction results obtained using the k–ϵ model are found to be very sensitive to the grid spacing, and a careful grid refinement study is presented in Figs. 3 and 4. Starting with the 120×110 grid, the numbers of points in the wall-normal direction are successively increased. A minimum of 200 points is found to be required to obtain a grid-converged solution. Next, the grid in the streamwise direction is refined. The skin friction coefficient on the ramp is found to change very little between the two finer grids (170×200 and 220×200). Based on these results, the 170×200 grid was used for all the k–ϵ simulations. Grid refinement results for the 20-deg and 16-deg compression corner flows were found to be identical to those shown above for the 24-deg case and are not presented.

Table 1 Freestream conditions and characteristics of the incoming turbulent boundary for the compression ramp flows

	Ramp angle, deg		
Parameter	24	20	16
Mach number	2.84	2.80	2.85
Freestream temperature, K	100.3	102.3	102.1
Freestream density, kg/m^3	0.83	0.88	0.82
Freestream velocity, m/s	570	568	578
Wall temperature, K	276.1	273.9	282.0
Reynolds number, 10^7 m^{-1}	6.8	7.0	6.7
Boundary layer thickness, m	0.024	0.025	0.026
Momentum thickness, m	0.0012	0.0013	0.0013

Simulation Results

The standard k–ω, k–ϵ, and SA models, as well as the models with shock-unsteadiness modification, are used in the simulations. Experimental measurement of surface pressure, skin friction coefficient, and mean velocity profiles at several streamwise locations

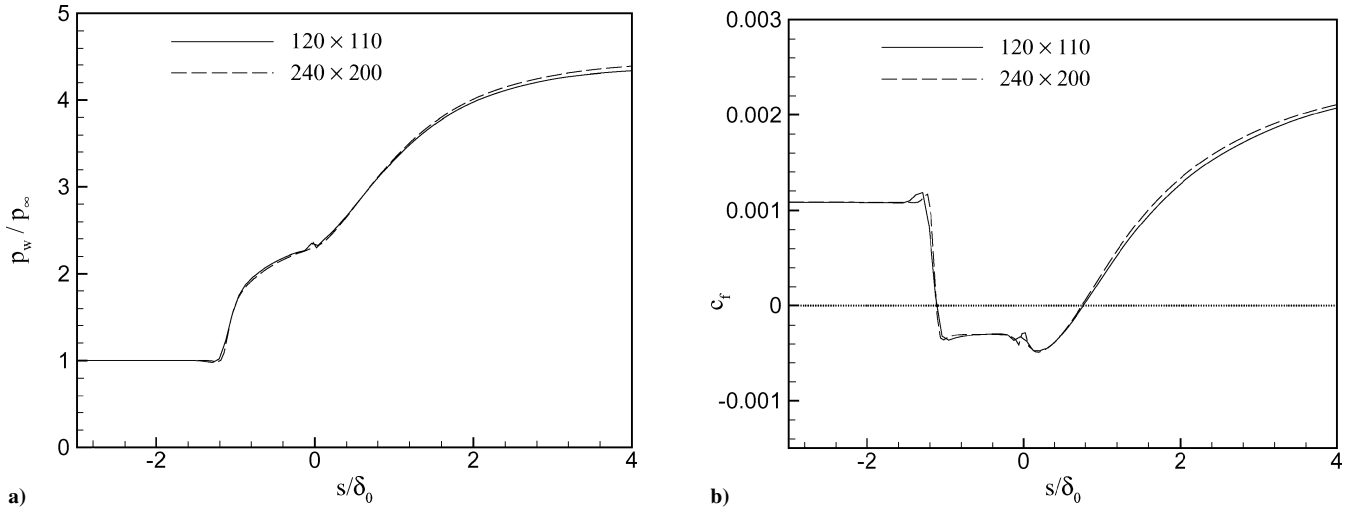

Fig. 1 Effect of grid refinement on a) normalized surface pressure and b) skin friction coefficient along a 24-deg compression corner obtained using the standard k–ω model.

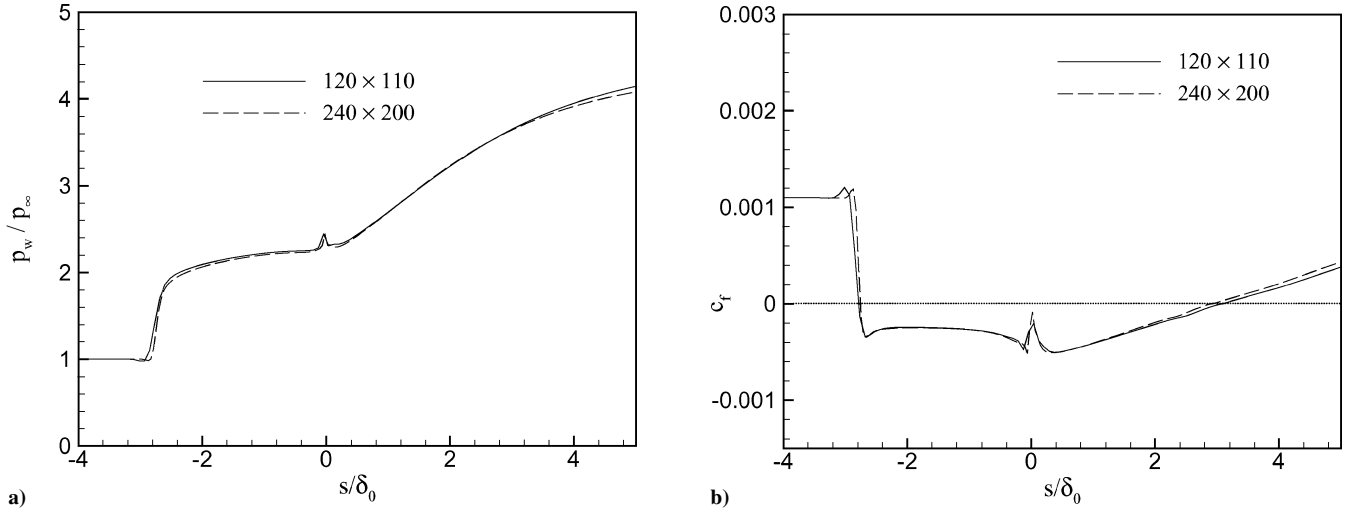

Fig. 2 Effect of grid refinement on a) normalized surface pressure and b) skin friction coefficient along a 24-deg compression corner obtained using the standard SA model.

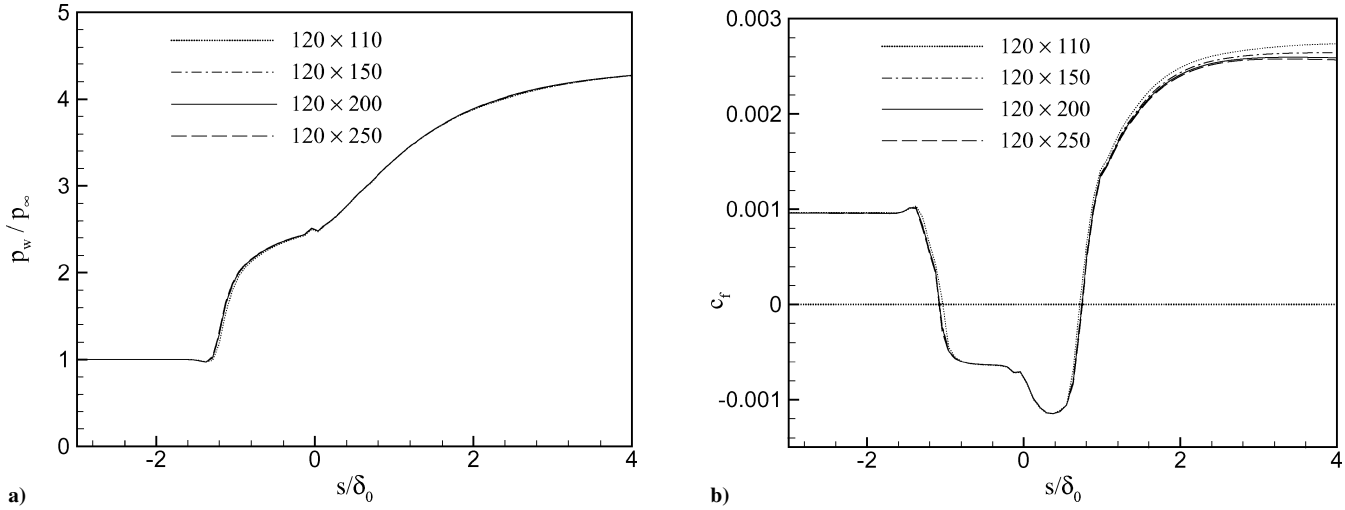

Fig. 3 Variation of a) normalized surface pressure and b) skin friction coefficient along a 24-deg compression corner obtained using the standard k–ϵ model on grids with varying number of points in the wall-normal direction.

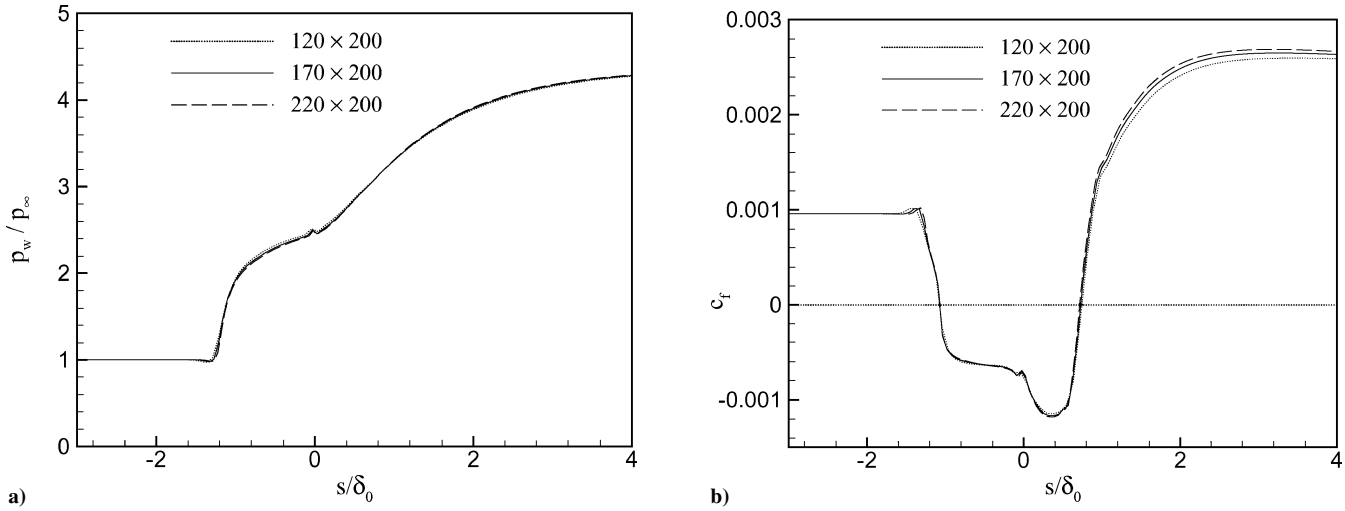

Fig. 4 Variation of a) normalized surface pressure and b) skin friction coefficient along a 24-deg compression corner obtained using the standard k–ϵ model on grids with varying numbers of points in the streamwise direction.

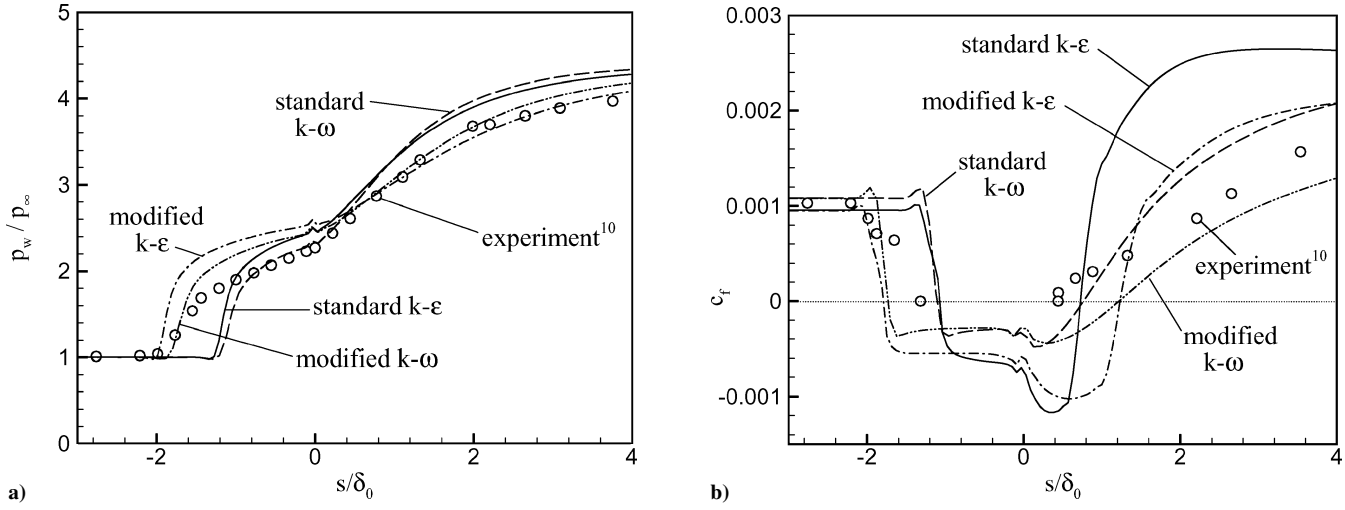

Fig. 5 Comparison of a) normalized surface pressure and b) skin friction coefficient along a 24-deg compression corner obtained using the standard and modified k–ω and k–ϵ models with experimental data.

in these flows are presented by Settles and Dodson.[10] The standard k–ω and k–ϵ model results show similar trends, and the effect of the shock-unsteadiness correction is comparable in these two models. Therefore, the simulations using the k–ω and k–ϵ models are described first. This is followed by the SA model results.

Simulation of 24-deg Compression Ramp

The normalized surface pressure distribution and the skin friction coefficient computed using the standard k–ω and k–ϵ models are shown in Fig. 5. Experimental data[10] are also plotted for comparison. The streamwise distance s along the plate and the ramp is normalized by the incoming boundary-layer thickness δ_0, where $s = 0$ represents the corner. The model results are similar to those reported in the literature.[2,14] Both models predict the separation shock location downstream of the experiment. The k–ω model matches the pressure plateau in the separation region, whereas the k–ϵ model overpredicts it by about 15%. The subsequent pressure rise on the ramp is also overpredicted by both models. The skin friction plot shows that the models predict a later separation than the experiment. The reattachment location is also downstream of the experimental data. The k–ϵ model greatly overpredicts c_f on the ramp, whereas the k–ω model predictions are higher than the measurements downstream of reattachment.

We apply the shock-unsteadiness correction to this flow. The modification is effective only in the separation shock as identified by the gray shaded region in Fig. 6, which corresponds to $S_{ii}/S < -0.3$. In the region of the shock wave that penetrates the incoming boundary layer ($y < \delta_0$), the Mach number normal to the shock varies between 1.3 and 1.6. $M_{1n} \simeq 1.3$ close to the wall and it attains higher values at the boundary-layer edge. The local value of M_{1n} is used to evaluate the damping parameter b_1' at each point in the shock. Note that M_{1n} is computed by taking a dot product of the streamwise Mach number in the incoming boundary layer with the pressure gradient vector in the shock wave:

$$M_{1n} = \frac{\tilde{\boldsymbol{u}}_1 \cdot \boldsymbol{\nabla} p}{a_1 |\boldsymbol{\nabla} p|}$$

where a_1 is the speed of sound upstream of the shock wave. Figure 7 shows the variation of k along a streamline originating at $y/\delta_0 = 0.2$ in the incoming boundary layer. The turbulent kinetic energy is normalized by its value upstream of the separation location. The standard k–ω model amplifies k by a factor of 2.8 across the separation shock (at $x \simeq -0.8\delta_0$), followed by a further increase in k in the shear layer enclosing the separated flow region at the corner. The highest value of k is attained in the reattachment region, and k decreases as the boundary layer recovers to an equilibrium state on the ramp. Using the shock-unsteadiness correction in the k–ω model, we get a much smaller increase in k across the separation shock at $x \simeq -1.5\delta_0$. This is because the shock-unsteadiness modification

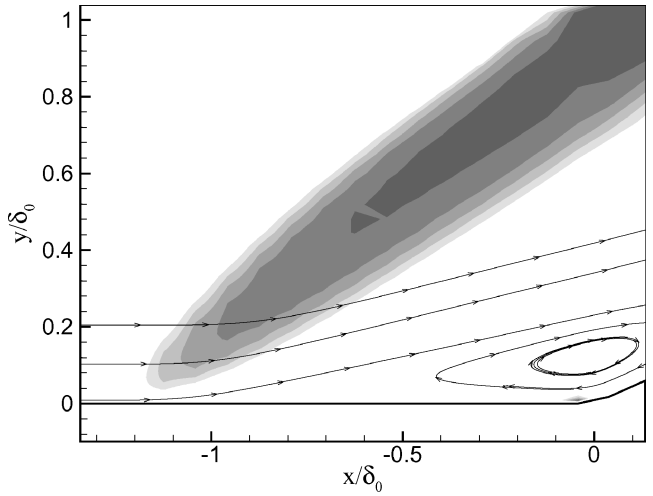

Fig. 6 Representative streamlines in the k–ω simulation of a 24-deg compression ramp flow. The gray region denotes the area where the shock-unsteadiness modification is active in the simulation.

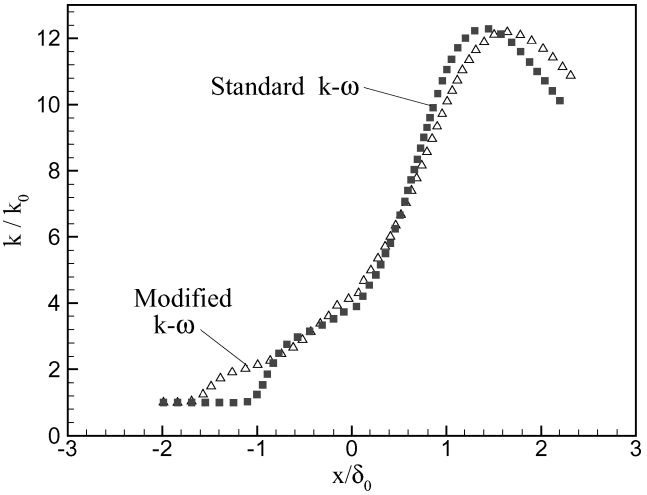

Fig. 7 Variation of turbulent kinetic energy along a streamline originating at $y/\delta_0 = 0.2$ in the k–ω simulation of a 24-deg compression ramp flow.

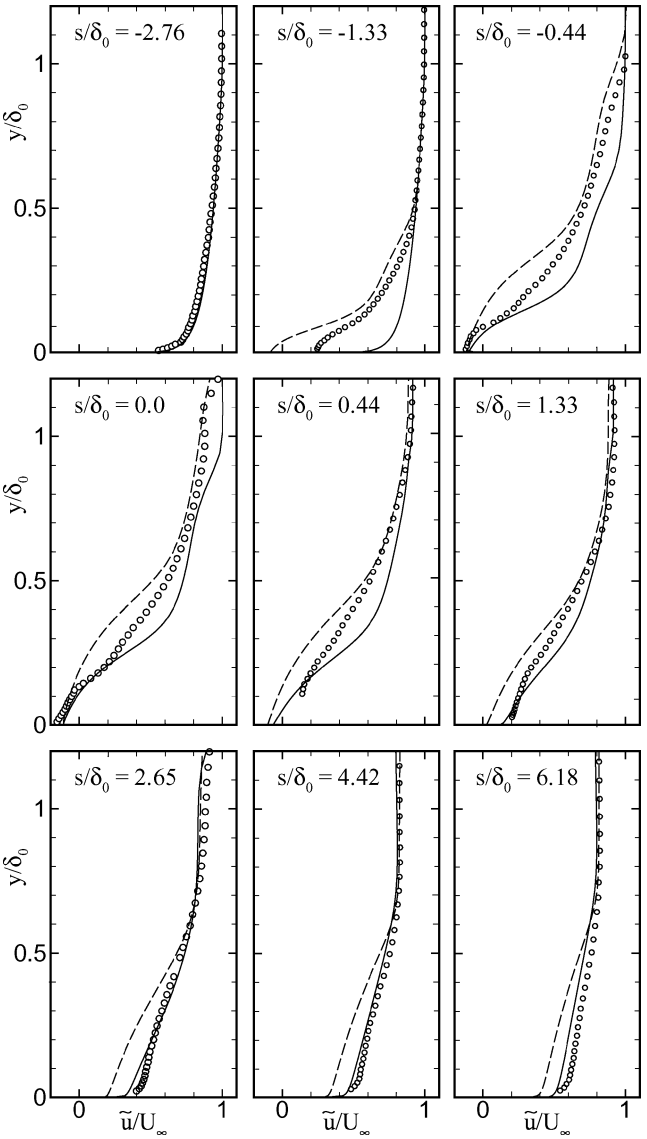

Fig. 8 Comparison of mean velocity profiles obtained using ——, the standard k–ω model and – – –, the shock-unsteadiness modification with ○, experimental data[10] in a 24-deg compression ramp flow.

reduces P_k substantially (maximum reduction 80%). Also, note that the evolution of k downstream of the shock is similar in both the standard and modified k–ω models. In the k–ϵ simulation of this flow, the variation of k along streamlines is similar to that shown in Fig. 7. The effect of the shock-unsteadiness modification in the k–ϵ model is also comparable to that in the k–ω model.

Lower amplification of k across the shock moves the separation point upstream and the model predictions match the experimental location of the pressure rise well (see Fig. 5a). The modification results in a pressure plateau higher than that in the corresponding standard model and reproduces the experimental pressure rise on the ramp accurately. The drop in c_f at $s \simeq -2\delta_0$, as predicted by the modified k–ω and k–ϵ models (see Fig. 5b), agree well with the experimental measurements, but the size of the separation region is overpredicted. Finally, the modification reduces c_f on the ramp as compared to the standard models.

The mean velocity profiles at different streamwise locations computed using the standard and modified k–ω models are shown in Fig. 8. Both models match the experimental data in the incoming boundary layer at $s/\delta_0 = -2.76$. The shock-unsteadiness correction results in better prediction of the velocity profiles near the separation location than the original k–ω model. Most notably, the outer parts of the boundary layer at $s/\delta_0 = -1.33$, -0.44, and 0 are reproduced well. However, the modification results in a larger recirculation region than the experiment, and therefore predicts lower velocity close to the wall. This also results in a slower recovery of the boundary layer on the ramp as compared to the standard k–ω model. Note that the velocity profiles obtained using the standard and modified k–ϵ models, not shown here, are very similar to those in Fig. 8.

As pointed out earlier, the Mach number normal to the shock varies between 1.3 and 1.6 in the region of the shock that penetrates the boundary layer. Using an intermediate value of $M_{1n} = 1.4$ to evaluate b_1' in the entire region of the shock wave yields results essentially identical to those obtained using the exact variation of M_{1n}. Also, there is very little sensitivity of the simulation results to the value of M_{1n} in the range $1.3 \leq M_{1n} \leq 1.6$.

Another way to suppress the amplification of turbulence across the shock is to use the realizability constraint, $0 \leq \widetilde{u_i'' u_i''} \leq 2k$. Different realizable models have been proposed in the literature. Here, we use the models presented by Durbin,[19] Thivet et al.,[20] and Shih et al.[21] to compute the 24-deg compression-corner flow. Note that the realizability corrections are modified by the wall-damping function f_μ corresponding to the Launder and Sharma k–ϵ model. The normalized pressure distribution and skin friction coefficient in Fig. 9 show that all the realizable models yield some improvement over the standard k–ϵ model. However, the results are highly dependent on the specific form of the realizability correction used. Durbin's model[19] moves the separation shock location upstream by a small amount, whereas the model by Thivet et al.[20] predicts the shock location far upstream of the experimental data. The realizable model by Shih et al.[21] is found to match the measured location of the separation shock and the onset of separation well (also see Ref. 2), and its prediction is similar to the k–ϵ model with shock-unsteadiness modification. The realizable models also predict lower c_f on the ramp than the standard model. Note that the production term in Eq. (2) satisfies the realizability constraint because the normal Reynolds stresses in the shock are modeled as $\frac{2}{3}\bar{\rho}k$ (obtained using $\mu_T = 0$).

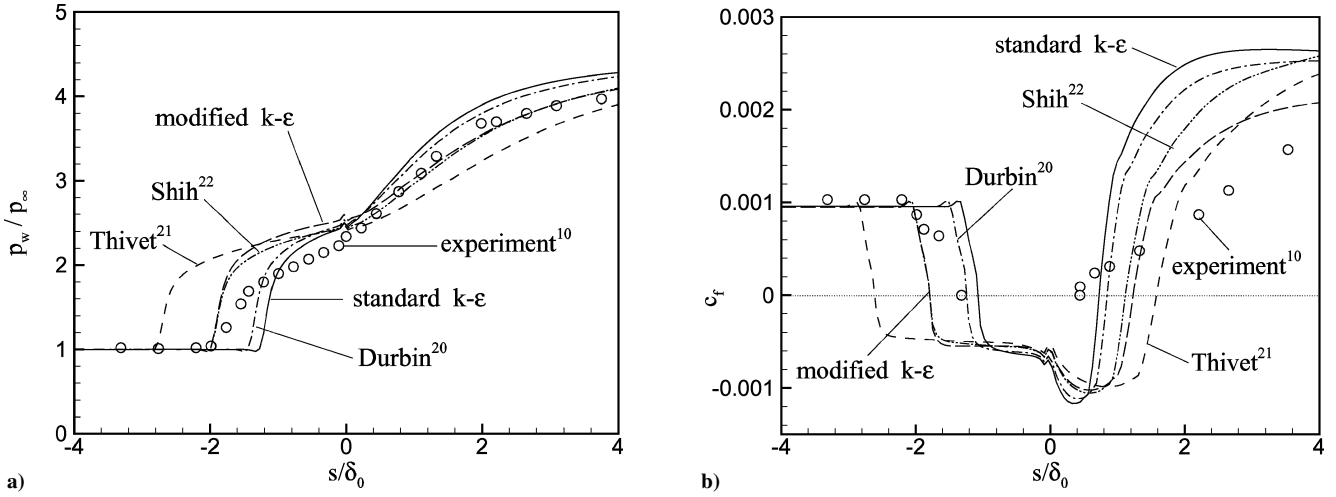

Fig. 9 Variation of a) normalized surface pressure and b) skin friction coefficient along a 24-deg compression corner obtained using the standard k–ϵ model and different realizable k–ϵ models.

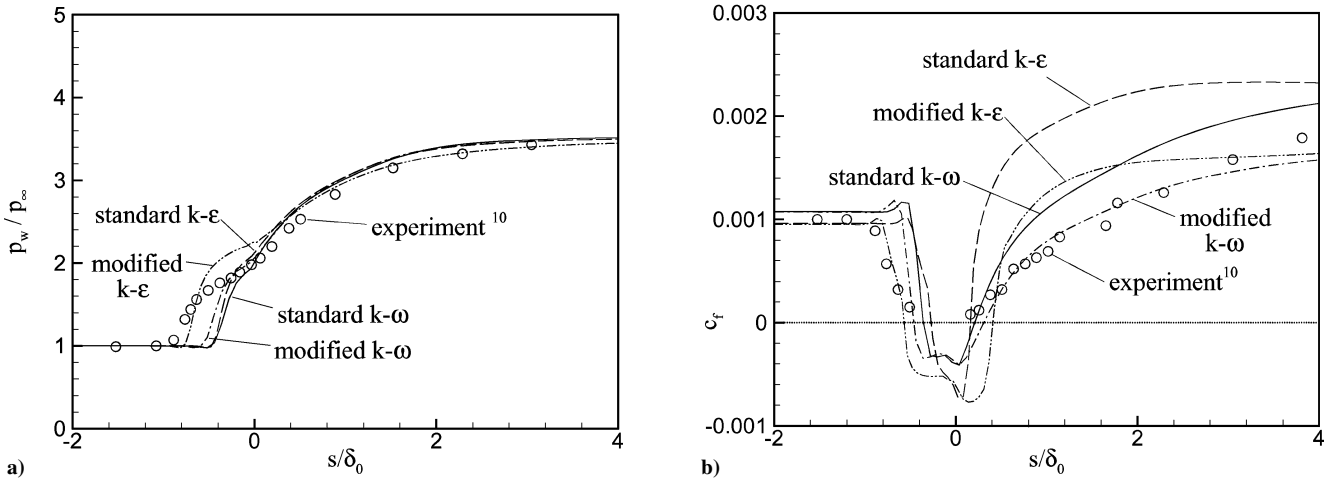

Fig. 10 Comparison of a) normalized surface pressure and b) skin friction coefficient along a 20-deg compression corner obtained using the standard and modified k–ω and k–ϵ models with experimental data.

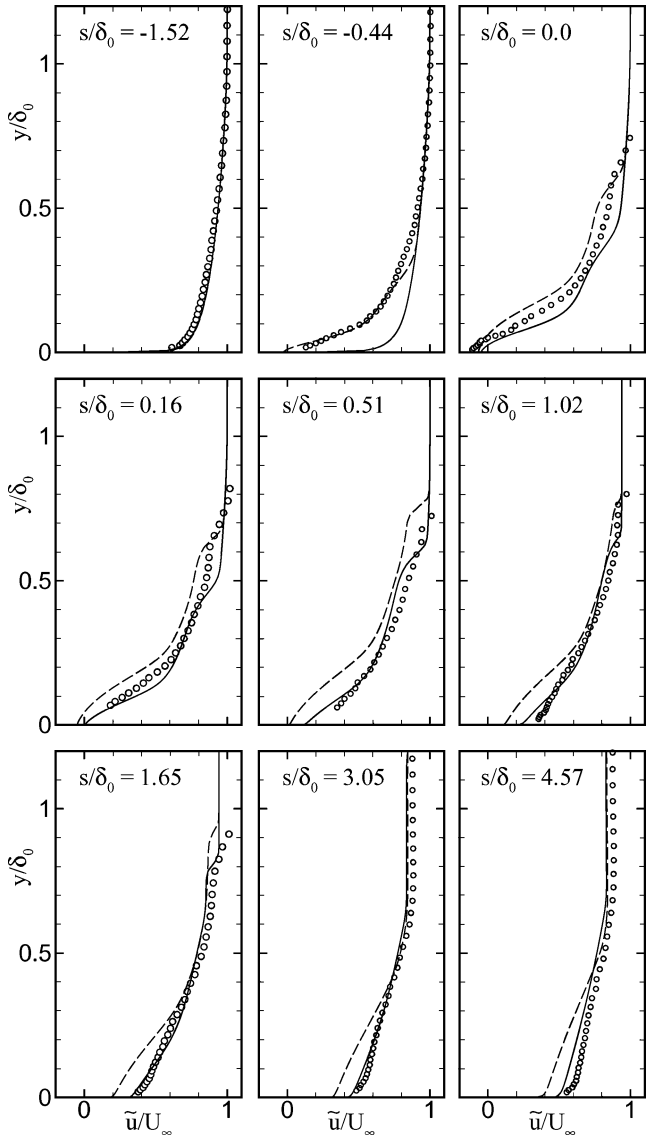

Fig. 11 Comparison of mean velocity profiles obtained using ——, the standard k–ϵ model and – – –, the shock-unsteadiness modification with ○, experimental data[10] in a 20-deg compression ramp flow.

Simulation of 20-deg Compression Ramp

We next apply the shock-unsteadiness modification to a 20-deg compression ramp flow. The upstream normal Mach number at the separation shock is found to vary between 1.3 and 1.5 in this flow. The simulation results are shown in Figs. 10 and 11 along with experimental data by Settles and Dodson.[10]

The location of the separation shock pressure rise as predicted by the standard k–ω and k–ϵ models is much downstream of the experimental data (Fig. 10a). The shock-unsteadiness correction moves the separation shock upstream. The effect of the modification is small in the k–ω simulation, whereas the modified k–ϵ model results are closer to the experimental separation shock location. Also, note that the modified k–ϵ model results in a higher pressure plateau in the separation region, similar to that in the 24-deg case. All of the models agree well with the pressure measurements on the ramp.

The skin friction data in Fig. 10b follow a pattern similar to that obtained in the 24-deg ramp flow. The standard k–ω and k–ϵ models predict a smaller separation region than in the experiment. By comparison, the shock-unsteadiness modification matches the measured separation location well for both the models. However, none of the models matches the decrease of c_f on the plate ($s \simeq -0.8\delta_0$). The correction also leads to later reattachment and a lower skin friction on the ramp as compared to the standard models. Note that the modified k–ω model matches the experimental skin friction on the ramp up to $s = 2.3\delta_0$.

The mean velocity profiles obtained using the standard and modified k–ϵ models are compared with experimental measurements in Fig. 11. The trends are similar to the 24-deg compression ramp flow presented earlier. The most significant improvement caused by the shock-unsteadiness modification is in the vicinity of the separation point. Specifically, at $s = -0.44\delta_0$, an attached boundary layer is obtained using the standard k–ϵ model, whereas the modification predicts separated flow that is close to the experimental data. The modified k–ϵ model also reproduces the location of the shock wave well, as seen in the velocity variation in the outer part of the boundary layer at the corner and at $s = 0.16\delta_0$. Finally, the correction results in a slower recovery of the boundary layer on the ramp. The k–ω model results, not shown here, are similar to those presented in Fig. 11, but the improvement caused by the shock-unsteadiness modification in the k–ω model is smaller than the k–ϵ results.

Simulation of 16-deg Compression Ramp

The flow over a 16-deg compression ramp is simulated using the standard and modified models, and the results are shown in Figs. 12 and 13. The computational domain and grid used in these simulations are very similar to those in the 24-deg case. An exception

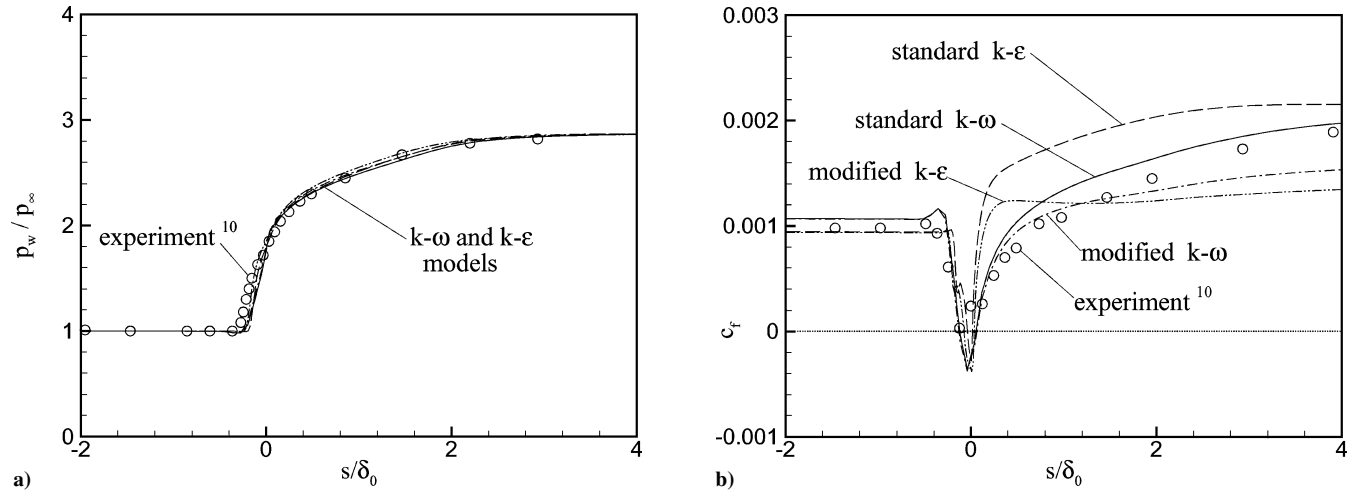

Fig. 12 Variation of a) normalized surface pressure and b) skin friction coefficient along a 16-deg compression corner obtained using the standard and modified k–ω and k–ϵ models.

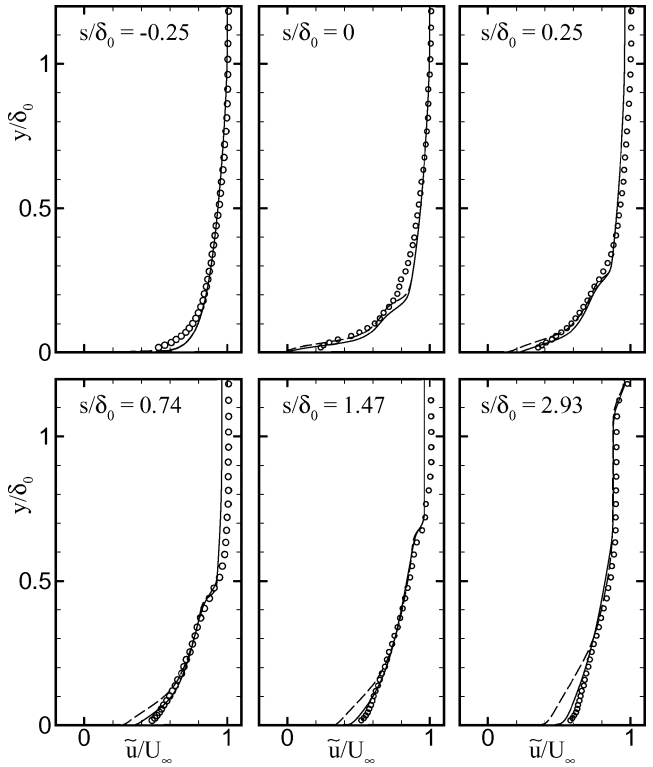

Fig. 13 Comparison of mean velocity profiles obtained using ——, the standard k–ϵ model and – – –, the shock-unsteadiness modification with ○, experimental data[10] in a 16-deg compression ramp flow.

is the k–ϵ simulation, which requires substantially higher resolution at the corner. Streamwise grid spacing of 0.2 mm in this region is used to reproduce a small separation region at the corner. M_{1n} is found to vary between 1.1 and 1.6 in the region of the shock wave.

The flow in this case is near incipient separation, so that the pressure variation (Fig. 12a) does not have the distinct pressure plateau that is observed at higher ramp angles. All of the models reproduce the experimental pressure measurements accurately, which points to the fact that the effect of the shock-unsteadiness correction on the pressure distribution is negligible for small ramp angles. The skin friction coefficient (Fig. 12b) shows a small region of separated flow at the corner. The standard and modified model results are identical on the plate ($s < 0$) that agree well with the experimental data. However, the model predictions differ in the recovery region on the ramp. The standard k–ϵ model overpredicts the skin friction, whereas the standard k–ω model matches the experimental data. The shock-unsteadiness modification results in lower c_f for both models. The mean velocity profiles in Fig. 13 show that both the standard and modified k–ϵ models agree well with the experimental data. There is a negligible effect of the shock-unsteadiness modification on the k–ϵ results, except for the near wall region on the ramp. The modified k–ϵ model yields a higher velocity deficit close to the wall than the standard model. The k–ω results show a similar trend.

Spalart–Allmaras Model Results

The effect of the shock-unsteadiness modification to the Spalart–Allmaras model is tested in a 24-deg compression corner flow (Table 1). The results are shown in Fig. 14. The standard SA model predicts the separation shock location significantly upstream of the experiment. The pressure plateau is overpredicted and the pressure on the ramp is lower than in the experimental data. The skin-friction coefficient drops below the flat plate value of 0.0011 at $s/\delta_0 \simeq -2.7$, which is upstream of the onset of separation in the experiment. The separation region is too large and c_f on the ramp is much lower than the experimental measurement. In the modified SA model, the production due to shock amplifies $\tilde{\nu}$ by 14% across the separation shock. Note that $1.3 < M_{1n} < 1.6$ yields c'_{b1} between 0.18 and 0.32

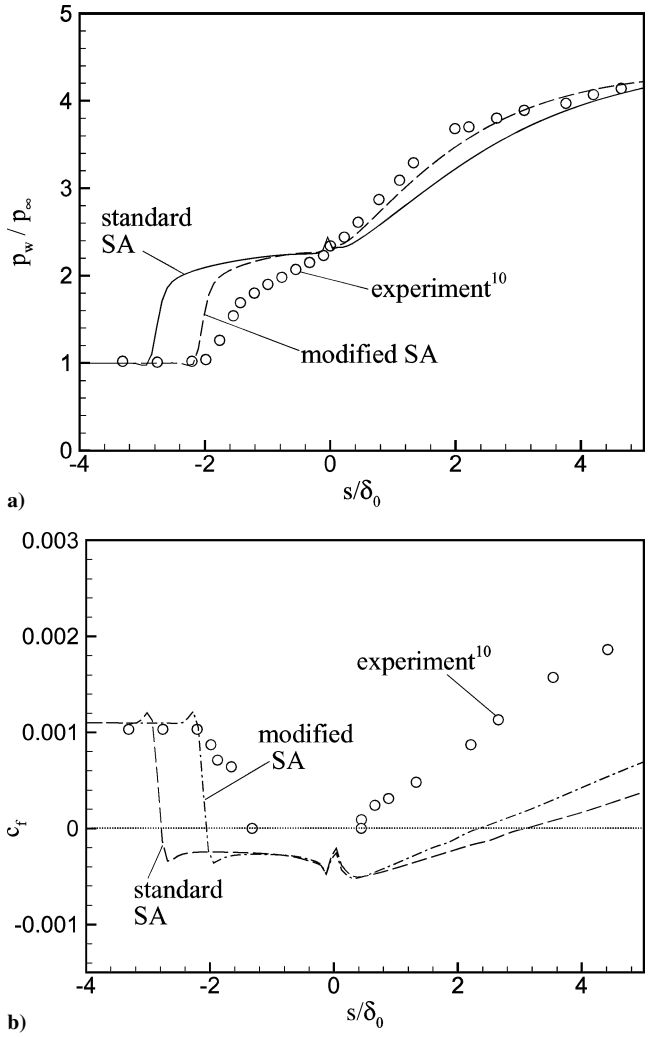

Fig. 14 Variation of a) normalized surface pressure and b) skin friction coefficient along a 24-deg compression corner obtained using the standard and modified SA models.

in this flow. Higher turbulent viscosity moves the separation point much closer to the experiment. The modification also increases c_f on the ramp by a small amount, but the results are significantly lower than the measurements.

Conclusions

In this paper, we generalize the shock-unsteadiness modification proposed by Sinha et al.[6] and apply it to k–ϵ, k–ω, and Spalart–Allmaras turbulence models. The effect of the correction is evaluated in compression-corner flows with deflection angles of 24, 20, and 16 deg, for which experimental data are provided by Settles and Dodson.[10] Standard k–ϵ and k–ω models predict later separation in these flows than found in the experiments, which may be caused by excessive amplification of the turbulent kinetic energy, k, through the separation shock. The shock-unsteadiness modification damps the amplification of k through the shock and results in earlier separation, which matches experimental data better than the standard models. However, the correction delays reattachment and results in an overly slow recovery of the boundary layer on the ramp. Also, the effect of the correction is found to decrease with the deflection angle so that it does not alter the separation location over low ramp angles where the standard models perform satisfactorily. In the Spalart–Allmaras model, the modification amplifies eddy viscosity across the shock that moves the separation location closer to the experiment. Both the standard and modified SA models yield low values of the skin friction coefficient on the ramp. Thus, whereas there remain some differences from experimental data, the proposed correction noticeably improves model predictions.

Acknowledgments

We acknowledge support from the Air Force Office of Scientific Research under Grant F49620-01-1-0060. This work was also sponsored by the Army High Performance Computing Research Center under the auspices of the Department of the Army, Army Research Laboratory cooperative agreement DAAD191-01-2-0014. The content of this report does not necessarily reflect the position or the policy of the government, and no official endorsement should be inferred. A portion of the computer time was provided by the University of Minnesota Supercomputing Institute.

References

[1]Knight, D., Yan, H., Panaras, A., and Zheltovodov, A., "RTO WG 10: CFD Validation for Shock Wave Turbulent Boundary Layer Interactions," AIAA Paper 2002-0437, Jan. 2002.

[2]Liou, W. W., Huang, G., and Shih, T.-H., "Turbulence Model Assessment for Shock Wave/Turbulent Boundary Layer Interaction in Transonic and Supersonic Flows," *Computers and Fluids*, Vol. 29, No. 3, 2000, pp. 275–299.

[3]Forsythe, J., Hoffmann, K., and Damevin, H.-M., "An Assessment of Several Turbulence Models for Supersonic Compression Ramp Flow," AIAA Paper 98-2648, June 1998.

[4]Coakley, T. J., and Huang, P. G., "Turbulence Modeling for High Speed Flows," AIAA Paper 92-0436, Jan. 1992.

[5]Knight, D. D., and Dregrez, G., "Shock Wave Boundary Layer Interactions in High Mach Number Flows—A Critical Survey of Current Numerical Prediction Capabilities," AGARD Advisory Rept. 319, Vol. 2, 1998, pp. 1.1–1.35.

[6]Sinha, K., Mahesh, K., and Candler, G. V., "Modeling Shock Unsteadiness in Shock/Turbulence Interaction," *Physics of Fluids*, Vol. 15, No. 8, 2003, pp. 2290–2297.

[7]Launder, B. E., and Sharma, B. I., "Application of the Energy Dissipation Model of Turbulence to the Calculation of Flow near a Spinning Disc," *Letters in Heat and Mass Transfer*, Vol. 1, No. 2, 1974, pp. 131–138.

[8]Sarkar, S., Erlebacher, G., Hussaini, M. Y., and Kreiss, H. O., "The Analysis and Modelling of Dilatational Terms in Compressible Turbulence," *Journal of Fluid Mechanics*, Vol. 227, June 1991, pp. 473–493.

[9]Sarkar, S., "The Pressure-Dilatation Correlation in Compressible Flows," *Physics of Fluids A*, Vol. 4, No. 12, 1992, pp. 2674–2682.

[10]Settles, G. S., and Dodson, L. J., "Supersonic and Hypersonic Shock/Boundary Layer Interaction Database," *AIAA Journal*, Vol. 32, No. 7, 1994, pp. 1377–1383.

[11]Wilcox, D. C., *Turbulence Modeling for CFD*, DCW Industries, La Canada, CA, 1998, pp. 236–239.

[12]Wilcox, D. C., "Reassessment of the Scale Determining Equation for Advanced Turbulence Models," *AIAA Journal*, Vol. 26, No. 11, 1988, pp. 1299–1310.

[13]Spalart, P. R., and Allmaras, S. R., "A One-Equation Turbulence Model for Aerodynamic Flows," AIAA Paper 92-0439, Jan. 1992.

[14]Wilcox, D. C., "Supersonic Compression-Corner Applications of a Multiscale Model for Turbulent Flows," *AIAA Journal*, Vol. 28, No. 7, 1990, pp. 1194–1198.

[15]MacCormack, R. W., and Candler, G. V., "The Solution of the Navier–Stokes Equations Using Gauss–Seidel Line Relaxation," *Computers and Fluids*, Vol. 17, No. 1, 1989, pp. 135–150.

[16]Sinha, K., and Candler, G. V., "Convergence Improvement of Two-Equation Turbulence Model Calculations," AIAA Paper 98-2649, June 1998.

[17]Wright, M. J., Candler, G. V., and Bose, D., "Data-Parallel Line Relaxation Method for the Navier–Stokes Equations," *AIAA Journal*, Vol. 36, No. 9, 1998, pp. 1603–1609.

[18]Menter, F. R., "Two-Equation Eddy Viscosity Turbulence Models for Engineering Applications," *AIAA Journal*, Vol. 32, No. 8, 1994, pp. 1598–1605.

[19]Durbin, P. A., "On the k–3 Stagnation Point Anomaly," *International Journal of Heat and Fluid Flow*, Vol. 17, No. 1, 1996, pp. 89–90.

[20]Thivet, F., Knight, D. D., Zheltovodov, A. A., and Maksimov, A. I., "Importance of Limiting the Turbulent Stresses to Predict 3D Shock-Wave/Boundary-Layer Interactions," 23rd International Symposium on Shock Waves, Paper 2761, July 2001.

[21]Shih, T. H., Liou, W. W., Shabbir, A., Yang, Z., and Zhu, J., "A New k–ϵ Eddy Viscosity Model for High Reynolds Number Turbulent Flows," *Computers and Fluids*, Vol. 24, No. 3, 1995, pp. 227–238.

M. Sichel
Associate Editor